Particle Accelerators
1973, Vol. 5, pp. 161–169

ENERGY DEPOSITION AND ENERGY-DEPOSITION FLUCTUATIONS IN AN IONIZATION SPECTROMETER AND A TOTAL-ABSORPTION NUCLEAR-CASCADE COUNTER†

T. A. GABRIEL and K. C. CHANDLER
Oak Ridge National Laboratory, Oak Ridge, Tennessee 37830, USA

Calculations have been carried out to determine the energy deposition and energy-deposition fluctuations produced by incident 28-GeV/c protons on an ionization spectrometer. In obtaining the pulse-height characteristics of the spectrometer, the nonlinearity of the light pulses is taken into account by the use of Birks' law and is shown to be of importance. A discussion of the experimental difficulties encountered in locating the position of the initial proton interaction within the spectrometer is also presented. Similar calculated results on the energy deposition and energy-deposition fluctuations are presented for 8-GeV/c negative pions incident on an NaI(Tl) total-absorption nuclear-cascade (TANC) counter. Also included for 8-GeV/c incident negative pions is the laterally integrated energy deposition as a function of depth in a tin absorber. In general, the calculational approach used is shown to yield good agreement with the experimental data.

1. INTRODUCTION

A renewed interest in ionization spectrometers and total-absorption nuclear-cascade (TANC) counters, which can be used to determine the energy of incident hadrons, has occurred recently due to the planning and building of the new multi-GeV hadron accelerators around the world and to the continuing interest in the high-energy portion of the galactic and solar cosmic-ray hadron spectra. A realistic calculational approach to the calibration problem can yield valuable insight into further design and development. In the work reported here, calculations have been carried out to compare with the experimental data of Jones *et al.*[1] on the energy deposition and energy-deposition fluctuations produced by 28-GeV/c protons incident on an ionization spectrometer and of Hughes *et al.*[2] on the energy deposition and energy-deposition fluctuations produced by 8-GeV/c negative pions incident on an NaI(Tl) total-absorption nuclear-cascade (TANC) counter, so that for future applications the validity of the calculational approach will have been verified. Also included for 8-GeV/c incident negative pions is the laterally integrated energy deposition as a function of depth in a tin absorber.

† This research was funded by the U.S. Atomic Energy Commission under contract with the Union Carbide Corporation.

The method of calculation is discussed in Sec. 2 and the results are presented in Sec. 3.

2. METHOD OF CALCULATION

The three-dimensional, high-energy nucleon–meson transport code HETC[3] was used to obtain a detailed description of the nucleon and meson cascade produced in each of the energy-absorbing devices. This Monte Carlo code takes into account the slowing down of charged particles (via the continuous slowing-down approximation), the decay of charged pions and muons, nonelastic nucleon- and charged-pion-nucleus (excluding hydrogen) collisions (through the intranuclear-cascade-evaporation model[4] ($E \lesssim 3$ GeV) and the extrapolation-evaporation model[5] ($E \gtrsim 3$ GeV)), nonelastic nucleon- and charged-pion-hydrogen collisions (via the isobar model[6] ($E \lesssim 3$ GeV) and phenomenological fits to experimental data[7] ($E \gtrsim 3$ GeV)), elastic neutron-nucleus collisions ($E \lesssim 100$ MeV), and elastic nucleon- and charged-pion collisions with hydrogen. In most applications using HETC, nucleons are transported to 15 MeV and charged pions are transported to ~ 2 MeV, with negative pions being captured when they slow down to their cutoff energy. In the present application, neutrons below 15 MeV were assumed to deposit their energy at their point of origin. In

applications where the transport of the low-energy neutrons is important, the three-dimensional multigroup neutron and gamma-ray Monte Carlo transport code MORSE[8] or the three-dimensional neutron Monte Carlo transport code O5R[9] are used.

The source distribution for the electromagnetic-cascade calculation, i.e., photons from neutral-pion decay and electrons and positrons from muon decay, is provided by HETC. The transport of these particles was carried out using a modified version of the Monte Carlo code developed by Beck.[10] This code takes into account all of the significant electron-, positron-, and photon-interaction processes. The main modification to the code was made to include a more generalized geometry package so that a three-dimensional transport calculation could be performed. However, for all processes except Compton scattering, the products of an interaction are assumed to be emitted in the same direction as the particle producing the interaction. Since Beck's code is a one-media transport code, a modification was made in the ionization-spectrometer calculation to account for the thin plastic scintillator sheets that are located within the device. The correct dE/dx was used at the scintillator locations, but the cross sections at these locations were not modified and were assumed to be the same as the iron cross sections.

Gamma-rays from the decay of excited nuclides following a nuclear interaction are not transported in the present calculations but are assumed to have deposited their energy at their point of origin. This is a fairly good approximation since a large portion of the electromagnetic cascade source energy for the problems considered here results from neutral pions. Also, since most de-excitation photons are of low energy, they are rapidly absorbed by the media.

The nonlinearity of the light pulse (i.e., the light observed is not in direct proportion to the energy deposited) from the plastic scintillators used by Jones *et al.*[1] has been taken into account by the use of Birks' law[11]:

$$\frac{dL}{dx} = \frac{dE/dx}{1+kB\,dE/dx} \quad \text{or}$$

$$L(E_2)-L(E_1) = \int_{E_1}^{E_2} \frac{dE}{1+kB\,dE/dx}. \qquad (1)$$

The light curves corresponding to several particles at low energies are shown in Fig. 1 for $kB = 0.01$ g cm^{-2}/MeV. In the calculation, the light curves were extended to the maximum necessary energy. The ionization energy loss, dE/dx, used in evaluating Eq. (1), was taken from a program due to Chandler and Armstrong.[12] It has been assumed that for electrons and positrons a linear relation holds between the light observed and the energy deposited; i.e., $L = E$. This is a very good approximation for all electron energies above 0.1 MeV.

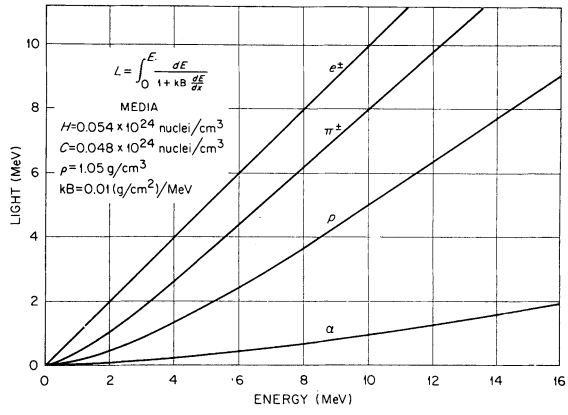

FIG. 1. Light output vs. energy for several different types of particles.

Neutrons with energies < 15 MeV are assumed to lose all their energy at their point of origin and to produce light in the scintillators through proton recoil. Since low-energy neutrons produce a small fraction of the light observed, this is a good approximation. In addition, the light produced by the residual excitation energy which remains in a nucleus following a nuclear interaction and which is emitted in the form of γ-rays is assumed to be directly proportional to the energy available.

The large NaI(Tl) crystals employed by Hughes *et al.*[2] exhibited a linear response[11] with respect to light output vs. energy deposited for particles of mass up to the deuteron. Therefore, since a majority of the energy deposited is from primary ionization, secondary proton and pion ionization, and the electromagnetic cascade, no correction for non-linearity was made for these calculations.

3. RESULTS

The Jones et al. Ionization Spectrometer

The material and dimensions of the ionization spectrometer used by Jones *et al.*[1] are shown in Fig. 2. The dimensions of each of the six iron slabs

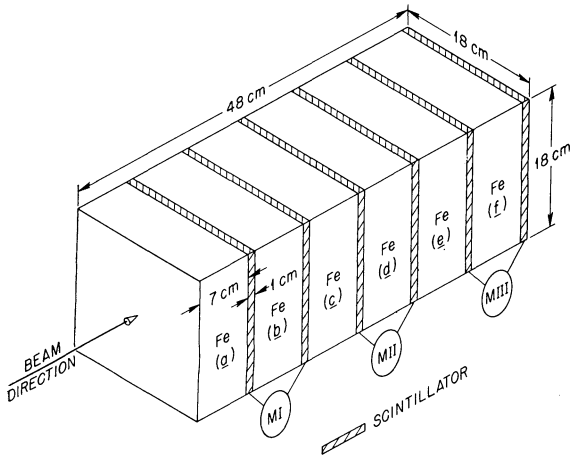

FIG. 2. Geometry and composition of the ionization spectrometer used in these calculations.

are $18 \times 18 \times 7$ cm^3 and those of each of the six plastic scintillators are $18 \times 18 \times 1$ cm^3. The incident 28-GeV/c protons were given the same spatial spread as measured experimentally,[1] and only those protons that entered the spectrometer within the spatial limits of $-4.5 \text{ cm} \leqq x \leqq 4.5$ cm and $-4.5 \text{ cm} \leqq y \leqq 4.5$ cm were considered.

The combined calculated and experimental results for the Jones *et al.* spectrometer are divided into two parts: The first part describes the results when no restriction on depth for the initial 28-GeV/c proton interaction is imposed, and the second part describes the results when the initial proton interaction is required to occur in the first (Fe(a)) iron slab.

1. *No restriction on depth for the initial proton interaction.* The calculated total-energy deposition and the individual contributions to the total deposition as a function of depth in the spectrometer are shown in Fig. 3. As can be seen from the figure, the major contributions to the total are from the primary and secondary protons, the secondary charged pions, and the electromagnetic cascade whose source energy comes from the decay of neutral pions and charged muons. In this application; neutrons with energies < 15 MeV, nuclear recoil fragments, evaporated charged particles with $A > 1$, and the photons from the residual excited nuclides which are produced in nuclear interactions are not transported and are assumed to deposit their energy at their point of origin. The peaks in the energy deposition show the location of the scin-

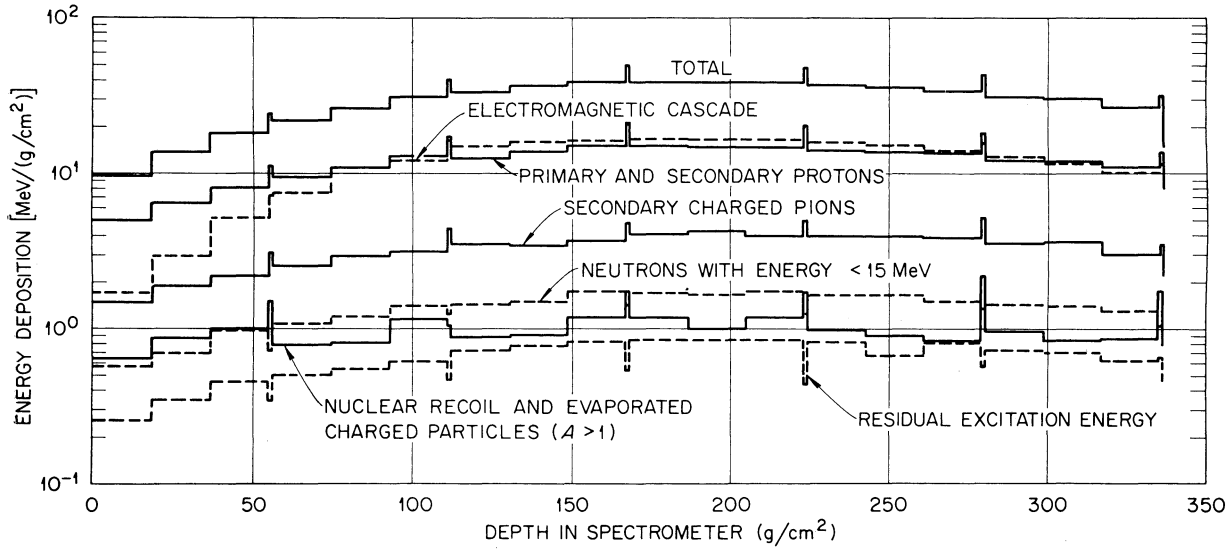

FIG. 3. Energy deposition in an ionization spectrometer by 28-GeV/c incident protons.

TABLE I

Individual contributions to the energy deposition and leakage by the interaction of 28-GeV/c protons in an ionization spectrometer

Type of energy deposition	Energy deposited (MeV)
Primary proton ionization	212.0
Secondary proton ionization	3,783.0
Secondary charged-pion ionization	1,100.0
Secondary muon ionization	12.5
Nuclear recoil and evaporated charged particles ($A > 1$)	317.0[a]
Residual excitation energy	224.0[a]
Neutrons with energy < 15 MeV	452.0[a]
Electromagnetic cascade	3,996.0
Total deposited	10,097.0

	Energy leakage from spectrometer (MeV)		
Particle type	Back	Front	Side
Protons	5,201.0	50.2	255.0
Neutrons	3,506.0	147.0	1,623.0
π^{+}[b]	1,328.0	95.5	196.0
π^{-}[b]	1,041.0	97.1	182.0
μ^{+}[b]	2.5	0.25	0.78
μ^{-}[b]	2.2	0.19	1.0
γ, e^{+}, e^{-}[b]	719.0	75.0	246.0
Total	11,800.0	465.0	2,503.0
Total leakage	14,768.0		
(Binding energy + ν energy) =	2,181.0		

[a] Assumed to deposit their energy at point of origin.
[b] Includes rest mass energy.

tillators and are produced by the larger dE/dx (MeV/g cm^{-2}) of the scintillators (see Sec. 2).

The individual contributors to the energy deposition, the leakage energy, and the binding energy plus neutrino energy are given in Table I.† The binding energy plus neutrino energy is obtained by an energy balance. As can be seen, less than 40 per cent of the incident energy on the average is retained by this spectrometer. The calculation also indicates that on the average less than 1 per cent of the incident energy is retained by the scintillators.

Because of the fluctuating nature of the nuclear and electromagnetic cascades in the spectrometer, the energy deposited in, or the light output from, the scintillators will not necessarily be the same for each incident particle at a fixed energy. These fluctuations are a direct consequence of the many reaction channels open not only for the incident particle but also for all secondary particles produced and of the leakage and binding energies. By forming a frequency distribution of the light pulses, the resolution of the device can be obtained, as well as the relationship between the incident energy and the average light pulse.

The frequency distribution of the light pulses for 28-GeV/c incident protons for the Jones *et al.* spectrometer is given in Fig. 4. All data have been normalized to the same area. In forming the scale for the particle axis for both the calculated and experimental data, the *average* light pulse from each consecutive pair of scintillators (see Fig. 2) was summed and the sum was divided by the light pulse of a standard particle. In these calculations, a standard particle is defined by 2.16 MeV/particle/cm (see footnote in Table III), which corresponds to the energy loss of a relativistic muon of ~ 700 MeV in kinetic energy transversing 1 cm of plastic

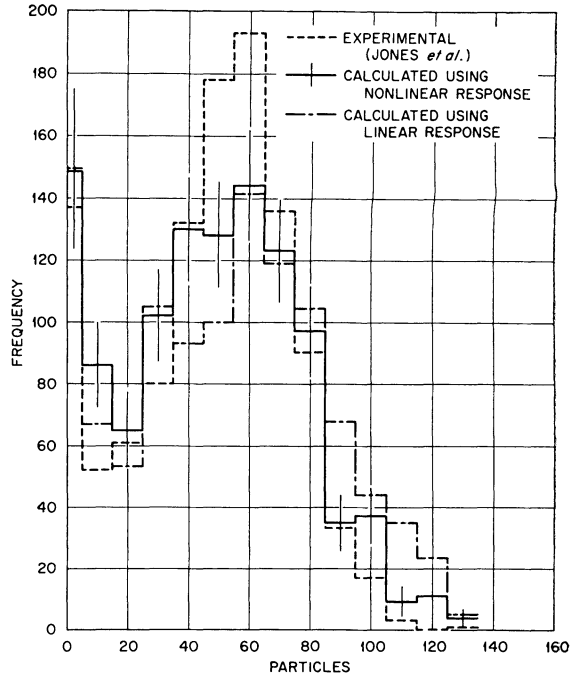

FIG. 4. Frequency distribution of the particle pulses from an ionization spectrometer irradiated by 28-GeV/c incident protons.

† The number of significant numbers shown in this table and in similar subsequent tables generally exceed the statistical accuracy of the calculation. In most instances, statistical error associated with the numbers is 5 per cent or less.

scintillator. Experimentally, the standard particle was arrived at by obtaining the most probable light pulse from sea-level muons which completely transversed the scintillator and by multiplying this most probable value by 1.15[1] to obtain the average.

The dashed histogram in Fig. 4 represents the experimental data and the solid histogram represents the calculated data obtained with the nonlinear response function defined by Eq. (1). The remaining histogram defines the calculated values obtained assuming a linear response. The effect of the nonlinearity can be easily seen by comparing the two calculated distributions. The large peak from 0 to 5 particles results mainly from those incident protons that transverse the entire scintillator without interacting.

The agreement between the calculated and experimental data is only fair, but this was not unexpected since the contamination of the experimental beam was estimated to be between 10 and 30 per cent.[1] Most of the contamination was from secondary-particle production in a target located directly in front of the spectrometer.

2. *Initial proton interactions occurring in the first iron layer.* The total spatial energy deposition and the nuclear and electromagnetic components of the total for only those incident 28-GeV/c protons that interact in the first iron layer are shown in Fig. 5. A further breakdown of the individual contributions to the energy deposition is given in Table II. In comparing the results in Table II with

TABLE II

Individual contributions to the energy deposition and leakage by the interaction of 28-GeV/c protons in the top iron layer of the spectrometer

Type of energy deposition	Energy deposited (MeV)
Primary proton ionization	49.0
Secondary proton ionization	4,864.0
Secondary charged-pion ionization	1,416.0
Secondary muon ionization	14.9
Nuclear recoil and evaporated charged particles ($A > 1$)	401.0[a]
Residual excitation energy	288.0[a]
Neutrons with energy < 15 MeV	585.0[a]
Electromagnetic cascade	4,843.0
Total deposited	12,461.0

	Energy leakage from spectrometer (MeV)		
Particle type	Back	Front	Side
Protons	2,240.0	125.0	428.0
Neutrons	2,976.0	283.0	2,199.0
π^{+}[b]	962.0	182.0	263.0
π^{-}[b]	781.0	172.0	256.0
μ^{+}[b]	3.0	0.35	1.3
μ^{-}[b]	2.3	0.29	1.3
γ, e^{+}, e^{-}[b]	349.0	239.0	332.0
Total	7,312.0	1,002.0	3,480.0
Total leakage	11,795		
(Binding energy + ν energy) =	2,790		

[a] Assumed to deposit their energy at point of origin.
[b] Includes rest mass energy.

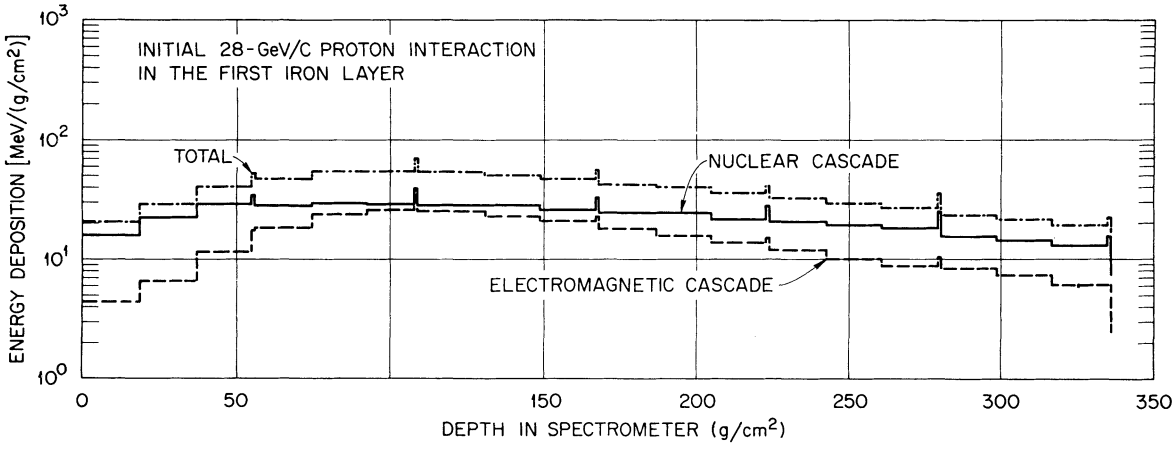

FIG. 5. Energy deposition in an ionization spectrometer by 28-GeV/c incident protons that interact in the top layer of the spectrometer.

those in Table I, it can be seen that the average amount of energy contained within the spectrometer has been increased. This fact is used in practice to increase the resolution of spectrometers but at a price of decreased efficiency.

The frequency distribution of the light pulses that result from 28-GeV/c protons interacting in the 'first' iron block is given in Fig. 6. The dashed histogram represents the experimental data and the solid histogram represents the calculated data obtained using the nonlinear response. The remaining histogram represents the calculated data obtained assuming a linear response. The agreement with the experimental data is good. The average number of particles, the average number of particles from each pair of scintillators, and the average maximum considering each pair of scintillators are given in Table III. The results are in good agreement with the experimental data.

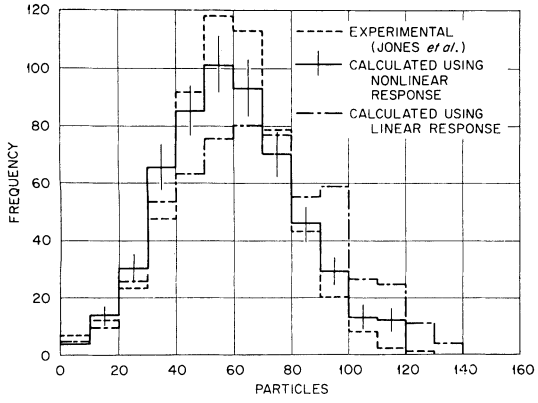

FIG. 6. Frequency distribution of the particle pulses from an ionization spectrometer irradiated by 28-GeV/c incident protons. The calculation treats the initial proton interaction as occurring in the first iron layer (see text).

TABLE III

Comparison of calculated and measured number of particles

	Calculated	Experimental
Average number of particles	59.3[a]	58.3
Average number of particles for the scintillator pairs:		
M I	28.9	30.4
M II	20.2	18.8
M III	10.2	9.0
Average maximum number of particles	33.7	35.5

[a] The energy loss of a standard particle in these calculations was chosen such that the average particle pulse would agree reasonably well with the corresponding experimental value. However, the energy loss of a standard particle in this paper, 2.16 MeV/cm/particle in the scintillator or 1.62 MeV/g/cm^2/particle in iron, is very similar to the energy loss of a standard particle defined as $1.56\pm.07$ MeV/g/cm^2/particle in iron.[13] (The spectrometer described in Ref. 13 is similar to that used in the present set of calculations.)

To determine experimentally within a small degree of uncertainty whether or not the initial proton interaction occurred in the first iron slab is very difficult. The method used by Jones *et al.*,[1] also employed in the calculations, is as follows: low-level discriminators on the first two scintillators were set to correspond to ionization in the scintillators of two or more particles; i.e., the minimum light pulse required to activate the discriminator was set at twice that defined for a standard particle. If *both* discriminators were activated, then the initial interaction was assumed to have occurred in the first iron slab. In addition, and independent of the low-level discriminators, a high-level discriminator on the first scintillator was set to correspond to 13 or more particles. If this discriminator was activated, the initial interaction was assumed to have occurred in the first iron slab. As pointed out by Jones *et al.*[1] initial proton interactions, which actually occurred in the first iron slab, can be missed because of the requirements placed on the light output from the scintillators. It was calculated that 5.5 ± 1.0 per cent of the incident protons interacting in the first iron slab or 2.0 per cent of the incident particles† are missed because of the bias.

In addition, incident protons that initially interact in the remaining iron blocks can possibly activate the two low-level discriminators or the one high-level discriminator giving the impression that the initial interaction was in the first iron slab. The probabilities for these occurrences were calculated to be 63 ± 9 per cent for those incident protons interacting in the second iron slab (Fe(b)) or 14.6 per cent of the incident particles, 22 ± 6 per cent of the third iron slab (Fe(c)) or 3.2 per cent of the incident particles, 20 ± 7 per cent for the fourth iron slab (Fe(d)) or 1.9 per cent of the incident particles, and 0 per cent for the remaining two slabs. This

† Based on a nuclear mean free path of 125 g/cm^2.

represents a net increase of 17.7 per cent. The large probability associated with the second iron slab is somewhat unexpected. However, it should be noted that both scintillators used to determine whether or not the first interaction occurs in the first iron slab encase the second iron slab.

The above probabilities are dependent upon the bias applied to the scintillators. An increase in the low-level bias will increase the 5.5 per cent probability while decreasing the remaining probabilities. This effect can be seen in Fig. 7. The ▲'s show the

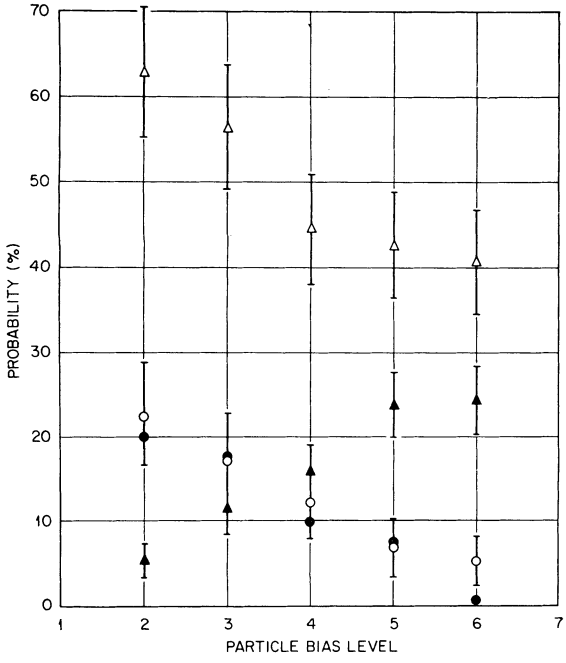

FIG. 7. Probability of rejecting an incident proton that interacted initially in the first iron layer because of the bias level (▲) or of accepting as interacting in the first iron layer an incident proton that initially interacted in the second iron layer (△), the third iron layer (○) or the fourth iron layer (●). For example, with a bias level of 4, 12% of the number of protons which interacted first in the third iron layer will appear to have interacted in the first iron layer. This is equivalent to 1.77% of the incident particles based on a nuclear mean free path of 125 g/cm².

increasing probability, as the bias increases, of rejecting a proton that interacted initially in the first iron slab, whereas the △'s, ○'s, and ●'s show the decreasing probabilities, as the bias increases, of accepting a proton, which actually interacted first in one of the deeper slabs, as initially interacting in the first iron slab. The probabilities given in Fig. 7 are not directly additive and must be converted to percent of incident particles before adding. It is evident from the magnitude of these probabilities that a substantial number of secondary particles is being emitted into the backward direction. Since the scaling model has not been completely verified in the backward angles due to a lack of experimental data, the data represented by the △'s, ○'s, and ●'s must be considered somewhat approximate.

The calculated histograms in Fig. 6 for 'Fe(a) interactions only' include all those initial proton interactions that appear to have originated in the first iron slab. Without the inclusion of the false Fe(a) interactions, the agreement with the experimental data is not nearly as good.

The Hughes et al. TANC Counter

Large NaI(Tl) crystals are also being used to determine the energy of strongly interacting particles in the GeV energy range. This type of detector has an advantage over the sandwich-type detector employed by Jones *et al.*[1] in that it can view a larger portion of the incident energy. Because of the smaller average density, however, the size of the detecting system must be made considerably larger if a significant portion of the incident energy is contained.

The NaI(Tl) crystals used by Hughes *et al.*[2] to determine the pulse-height characteristics for incident 8-GeV/c negative pions consisted of 11 crystals ranging in size from $9\frac{3}{8}$ to $13\frac{1}{2}$ in. in diameter and from $3\frac{3}{4}$ to 7 in. thick with a total average dimension of $11\frac{1}{2}$ by 56 in. In obtaining the calculated results, the exact experimental geometry was used. In the calculation, the incident beam was assumed to be of zero width and to enter the device at the center of the front face.

The frequency distribution of the energy deposited (or light pulse) is shown in Fig. 8. The data have been normalized to the same area between the energy limits of 2.0 and 7.5 GeV. The jagged curve represents the experimental data. The large peaks at approximately 1 GeV are from incident muons (not included in the calculations) and from a few incident 8-GeV/c negative pions which transverse the entire device without interacting. The peak at 8 GeV is produced by incident 8-GeV/c electrons (not included in the calculations), which were used for

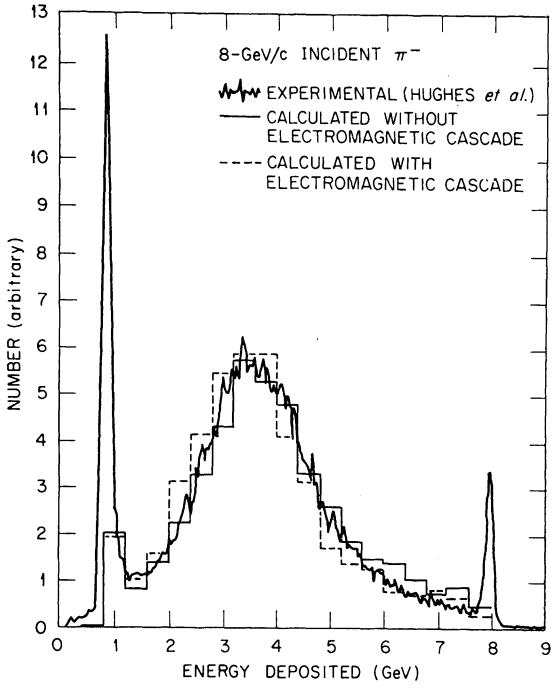

FIG. 8. Energy-deposition fluctuation in a TANC counter irradiated by 8-GeV/c negative pions.

calibration purposes. The solid histogram gives the calculated data in which it is assumed that the electron–photon cascade source energy, i.e., the neutral pions, and the electrons and positrons from muon decay, is deposited at its point of origin. The dashed histogram represents the calculated data with the electromagnetic transport included. As can be seen, there is some leakage from the electromagnetic cascade. The agreement with the experimental data is quite good. Hughes *et al.* calculated the average containment energy to be 49 per cent. The calculated containment energy for the two cases shown in Fig. 7 and discussed above is 50 per cent and 46 per cent, respectively.

TABLE IV

Individual contributions to the energy deposition and leakage by the interaction of 8-GeV/c negative pions in a TANC counter

Type of energy deposition	Energy deposited (MeV)
Primary negative-pion ionization	267.0
Secondary proton ionization	1,044.0
Secondary charged-pion ionization	407.0
Secondary muon ionization	4.9
Nuclear recoil and evaporated charged particles ($A > 1$)	124.0[a]
Residual excitation energy	70.0[a]
Neutrons with energy < 15 MeV	261.0[a]
Electromagnetic cascade	1,508.0
Total deposited	3,686.0

	Energy leakage from spectrometer (MeV)		
Particle type	Back	Front	Side
Protons	122.0	21.8	322.0
Neutrons	276.0	103.0	1,264.0
π^{+}[b]	69.1	28.3	201.0
π^{-}[b]	40.5	38.5	403.0
μ^{+}[b]	0.62	0.18	1.7
μ^{-}[b]	6.34	0.12	3.2
γ, e^{+}, e^{-}[b]	29.9	36.9	190.0
Total	544.0	229.0	2,385.0
Total leakage	3,156.0		
(Binding energy + ν energy) = 1,158.0			

[a] Assumed to deposit their energy at point of origin.
[b] Includes rest mass energy.

A breakdown of the energy deposition and

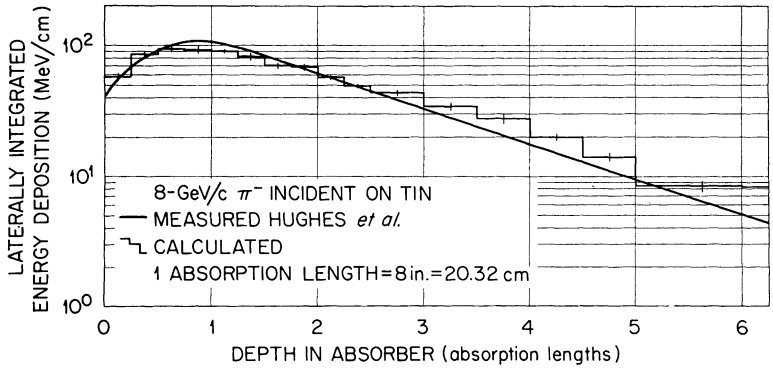

FIG. 9. Laterally integrated energy deposition in a tin absorber by 8-GeV/c incident negative pions.

leakage, similar to that shown in Tables I and II, is given in Table IV.

In addition to measuring the energy fluctuation in large NaI(Tl) crystals, Hughes *et al.* measured the spatial dependence of the energy deposition in tin produced by incident 8-GeV/c negative pions. The geometry of the absorber in both the calculation and in the experiment was 12 in. wide by 12 in. high by 30 in. long. In the calculation, the incident beam entered the absorber at the center of the front face. Tin was chosen for the experiment because of its similarity to iodine. The laterally integrated energy deposition is shown in Fig. 9 as a function of depth in the absorber. The absorption length used in obtaining the depth was taken from Ref. 2.

Since the experimental data were arbitrarily normalized, these results have been normalized to the calculated data. In general, the agreement in shape is good.

4. CONCLUSIONS

The calculational methods presented in this paper yield reasonable results when compared to experimental data and can be used to complement the designing and calibrating of ionization spectrometers and TANC counters. There is a large amount of detailed information which can be obtained through the use of the Monte Carlo codes described in this paper and which can be used to design better devices. Much of this information, which for the most part is very difficult if not impossible to obtain experimentally, may be obtained very readily.

ACKNOWLEDGEMENTS

The authors wish to thank Dr. R. G. Alsmiller, Jr. ánd Dr. T. W. Armstrong of the Oak Ridge National Laboratory, Dr. M. Awschalom of the National Accelerator Laboratory, and Dr. W. V. Jones of Louisiana State University for many helpful comments and discussions. Additional thanks are due to Dr. Armstrong who implemented many of the initial modifications in the electron–photon transport code. We also wish to extend our gratitude to Phillip R. Coleman and John D. Amburgey of the Oak Ridge National Laboratory for programming and calculating the light response curve.

REFERENCES

1. W. V. Jones *et al.*, *Nucl. Instr. Meth.*, **72,** 173 (1969).
2. E. B. Hughes *et al.*, *Nucl. Instr. Meth.*, **75,** 130 (1969).
3. K. C. Chandler and T. W. Armstrong, 'Operating Instructions for the High-Energy Nucleon–Meson Transport Code HETC,' Oak Ridge National Laboratory Report ORNL-4744 (1792).
4. H. W. Bertini, *Phys. Rev.*, **C6,** 631 (1972).
5. T. A. Gabriel, R. G. Alsmiller, Jr., and M. P. Guthrie, 'An Extrapolation Method for Predicting Nucleon and Pion Differential Production Cross Sections from High-Energy (> 3 GeV) Nucleon–Nucleus Collisions,' Oak Ridge National Laboratory Report ORNL-4542 (1970).
6. Hugo W. Bertini, Miriam P. Guthrie, and Arline H. Culkowski, 'Phenomenologically Determined Isobar Angular Distributions for Nucleon–Nucleon and Pion–Nucleon Reactions Below 3 GeV,' Oak Ridge National Laboratory Report ORNL-TM-3132 (1970).
7. T. A. Gabriel, R. T. Santoro, and J. Barish, 'A Calculational Method for Predicting Particle Spectra from High-Energy Nucleon and Pion Collisions (≧ 3 GeV) with Protons,' Oak Ridge National Laboratory Report ORNL-TM-3615 (1971).
8. E. A. Straker *et al.*, 'The MORSE Code—a Multigroup Neutron and Gamma-Ray Monte Carlo Transport Code,' Oak Ridge National Laboratory Report ORNL-4585 (1970).
9. D. C. Irving *et al.*, 'O5R, a General-Purpose Monte Carlo Neutron Transport Code,' Oak Ridge National Laboratory Report ORNL-3622 (1965).
10. H. L. Beck, 'A Monte Carlo Simulation of the Transport of High-Energy Electrons and Photons in Matter,' USAEC Health and Safety Laboratory Report HASL-213 (1969).
11. J. B. Birks, *The Theory and Practice of Scintillation Counting* (The Macmillan Company, New York, 1964).
12. T. W. Armstrong and K. C. Chandler, 'SPAR, a FORTRAN Program for Computing Stopping Powers and Ranges for Muons, Charged Pions, Protons, and Heavy Ions,' Oak Ridge National Laboratory Report ORNL-4869 (in press).
13. Haven Whiteside *et al.*, 'Energy Calibration of a Cosmic Ray Ionization Spectrometer,' NASA Goddard Space Flight Center Report X-661-72-316 (1972).

Received 30 April 1973